

Thermo-optic switch based on transmission-dip shifting in a double-slot photonic crystal waveguide

Kaiyu Cui, Qiang Zhao, Xue Feng, Yidong Huang, Yongzhuo Li et al.

Citation: *Appl. Phys. Lett.* **100**, 201102 (2012); doi: 10.1063/1.4718353

View online: <http://dx.doi.org/10.1063/1.4718353>

View Table of Contents: <http://apl.aip.org/resource/1/APPLAB/v100/i20>

Published by the [American Institute of Physics](#).

Related Articles

Complementary cellophane optic gate and its use for a 3D iPad without glasses
Rev. Sci. Instrum. **83**, 043710 (2012)

A nanomachined optical logic gate driven by gradient optical force
Appl. Phys. Lett. **100**, 113104 (2012)

Thermo-optic plasmo-photonic mode interference switches based on dielectric loaded waveguides
Appl. Phys. Lett. **99**, 241110 (2011)

Short hybrid polymer/sol-gel silica waveguide switches with high in-device electro-optic coefficient based on photostable chromophore
AIP Advances **1**, 042137 (2011)

Liquid crystal-based dielectric loaded surface plasmon polariton optical switches
J. Appl. Phys. **110**, 093102 (2011)

Additional information on *Appl. Phys. Lett.*

Journal Homepage: <http://apl.aip.org/>

Journal Information: http://apl.aip.org/about/about_the_journal

Top downloads: http://apl.aip.org/features/most_downloaded

Information for Authors: <http://apl.aip.org/authors>

ADVERTISEMENT



Goodfellow
metals • ceramics • polymers • composites
70,000 products
450 different materials
small quantities fast

www.goodfellowusa.com

Thermo-optic switch based on transmission-dip shifting in a double-slot photonic crystal waveguide

Kaiyu Cui, Qiang Zhao, Xue Feng, Yidong Huang,^{a)} Yongzhuo Li, Da Wang, and Wei Zhang
*Department of Electronic Engineering, State Key Laboratory of Integrated Optoelectronics,
 Tsinghua University, Beijing 100084, China*

(Received 21 December 2011; accepted 30 April 2012; published online 14 May 2012)

Optical switch based on an ultra-compact double-slot photonic crystal waveguide (DS-PCWG) with a titanium/aluminum microheater is demonstrated. The operating principle relies on shifting a transmission-dip caused by the defect mode coupling in photonic band gap (PBG). Based on the unique mode coupling in PBG, low switching power of 9.2 mW and high extinction ratio of 17 dB are achieved experimentally while the length of DS-PCWG is only 16 μm . © 2012 American Institute of Physics. [<http://dx.doi.org/10.1063/1.4718353>]

To meet the growing demands of on/off-chip communications for future multiprocessors, network-on-chip (NoC) has been considered as a feasible solution.¹ For such applications, optical switch, as one of the essential elements for all routing functions, is required to be compact, low power, robust, and complementary metal-oxide-semiconductor (CMOS) compatible.^{2–4} Thus, the preponderant candidate is silicon based optical switches, which could be realized by thermo- or electro-optic effect. Compared with electro-optic switch, thermo-optic (TO) switch is promising due to larger refractive index variation offered by TO effect while the switching time of tens of microseconds^{3,5,6} is enough for routing operations.⁷ The main challenges for the TO switches in silicon are small footprint and low operating power. For this purpose, the interaction between light and silicon material should be enhanced. High Q microring resonator could be a solution, but it is very sensitive to thermal fluctuations or fabrication imperfections, and also the operating bandwidth is very narrow.^{5,8,9} Another one is photonic crystal waveguide (PCWG) with the help of slow light effect, which could be achieved with a flexible design of the photonic band structure.^{10–13} There are two operating mechanisms reported for the PCWG based optical switches. One is applying PCWGs on the conventional Mach-Zehnder interferometers (MZIs)^{5,6} or directional couplers,³ where PCWGs are used to realize π phase-shift with a small size, a low operating power. The other one is based on the cutoff effect in a single PCWG.^{14,15} Around the cutoff frequency at the edge of photonic band gap (PBG), there is an abrupt drop of the light transmission. By shifting the transmission dip, optical switch could be obtained. Obviously, switch based on the single PCWG is much simpler and more compact. However, the insertion loss of such switch based on the cutoff effect is also much higher due to the strong light reflectance at discontinuities of group index n_g , which would degrade the transmission extinction ratio and make the devices sensitive to fabrication imperfections.¹⁶ The reported extinction ratio for the switch with cutoff effect in PCWG is just about ~ 0.42 (~ 3.8 dB) while the applied current is 70 mA.¹⁵

In this paper, we experimentally demonstrate a different operating principle for PCWG switches by the unique coupling between the defect modes in PBG, which is realized by our previously proposed double-slot photonic crystal waveguide (DS-PCWG).¹⁷ The DS-PCWG is formed by introducing two slots into a W3 PCWG (a line-defect PCWG with three rows of holes missing). We find that there is a transmission-dip in the DS-PCWG due to the defect modes coupling. By shifting the transmission-dip, the TO switching phenomenon is observed by the fabricated DS-PCWG with a length of 16 μm and covered with titanium (Ti)/aluminum (Al) microheater. Compared with the PCWG used cut-off effect to realize switching functionality, typically W1 PCWG,^{14,15} the width of DS-PCWG is enlarged so that the coupling efficiency can be improved while a simple and compact structure could still be obtained. According to the experimental results, extinction ratio of 17 dB and switching power of 9.2 mW are achieved. Among the reported TO PCWG based switches to date, this extinction ratio is the highest while the power consumption is the lowest.

DS-PCWG with Ti/Al microheater was fabricated on silicon-on-insulator (SOI) substrate with a 230-nm thick silicon layer. The optical microscope picture of the fabricated DS-PCWG with the Ti/Al microheater is shown in Fig. 1(a), where an enlarged figure of the Ti microheater in reference to the DS-PCWG is shown in the right inset, and the corresponding area in the left figure is marked out. Figure 1(b) presents the scanning electron microscope (SEM) image of the DS-PCWG without the driving electrode. The lattice constant of the DS-PCWG (a) and the radius of the holes (r) are 400 and 130 nm, respectively. The slot width (W_{slot}) is 80 nm, and the center-to-center distance of the two slots (W) is 560 nm. The length of the DS-PCWG is 16 μm . On the top of the DS-PCWG, 1 μm thick SiO_2 overcladding layer was deposited to obtain both optical and electrical isolations.^{3,6} The cladding layer is also helpful to obtain vertical symmetric waveguide structure so that the end-fire coupling efficiency between the fiber and the access waveguide could be improved. Then, the microheater was fabricated as a right-angle bent Ti strip with width of 3 μm and thickness of 100 nm to obtain high heating efficiency and uniform temperature distribution. Additionally, two Al electrical contact

^{a)}Electronic mail: yidonghuang@tsinghua.edu.cn.

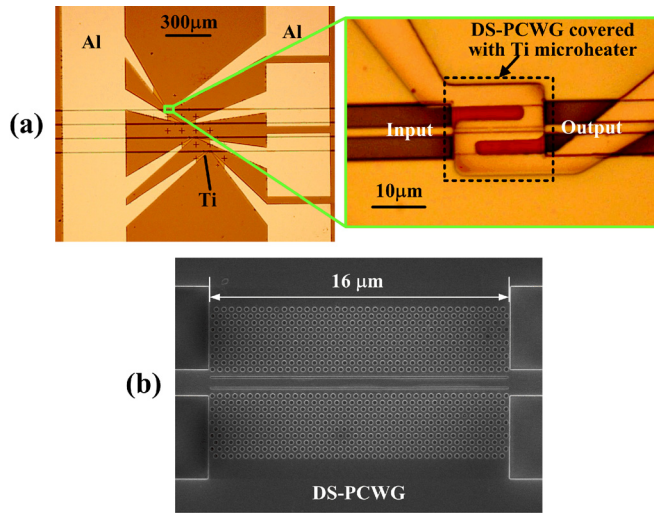


FIG. 1. (a) Microscope picture of the fabricated DS-PCWG with its titanium (Ti)/aluminum (Al) microheater, where an enlarged figure of the Ti microheater in reference to the DS-PCWG is shown in the right inset, and the corresponding area in the left figure is marked out; (b) SEM image of the DS-PCWG without the driving electrode. The lattice constant, a , and the hole radius, r , are 400 and 130 nm, respectively. The slot width, W_{slot} , is 80 nm, and the distance between the centers of the two slots, W , is 560 nm.

pads were deposited on the top and both sides of the Ti microheater to reduce the contact resistance, as marked in Fig. 1(a). The measured resistance of the whole micro-heater is 435 Ω .

The band structure and transmission spectra of the transverse electric (TE) mode were calculated by 2D plane wave expansion (PWE) method and 2D finite-difference time-domain (FDTD) method with setting effective refractive index of $n_{\text{eff}}=2.79$ while the structure parameters are consistent with the fabricated sample and shown in Fig. 2. The insets in Fig. 2(a) are magnetic field intensity patterns for the defect modes. Due to the unique guiding mechanism of PBG effect, PCWG offers the possibility to guide light in the line defect waveguide and Bragg couplings between the defect modes. It can be seen from Fig. 2(a) that there are mode couplings between the fundamental mode (#0) and the higher order mode (#2) so that in the frequency range of the fundamental mode, mini-gaps so-called mini-stopbands (MSB)¹⁸ appear.

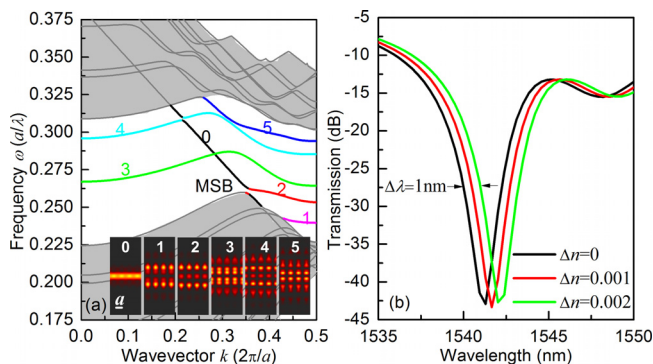


FIG. 2. (a) Band structure and magnetic field intensity patterns at $k=0.3$ for mode #0 and $k=0.5$ for the other higher order modes. (b) Transmission spectra under different refractive index variations of the transverse electric mode of the DS-PCWG with structure parameters consisting with the fabricated sample.

Different from the conventional coupling structures, such as MZIs, directional couplers, or distributed feedback (DFB) gratings, mode coupling in both W3 and DS PCWG originates from the interaction between defect modes in PBG. The defect modes are usually with lower group velocity v_g , namely, large group index n_g , which can be seen from its dispersion curve in Fig. 2, where $n_g = dk/d\omega$ ($v_g = c/n_g$). Therefore, mode coupling in both W3 PCWG and DS PCWG can be enhanced by the slow light effect.¹⁸ Furthermore, compared with W3 PCWG, the mode coupling in DS-PCWG can be enhanced as well due to that the slot structure changes the defect modes in PBG. Just as that shown in Fig. 2, mode coupling in DS-PCWG occurs between modes #0 and #2, while the mode coupling in W3 PCWG occurs between modes #0 and #4.^{13,18} It should be noted that the field of the lower order modes are concentrated more in the center of the waveguide and have larger overlap with the fundamental mode #0, which can be seen in the insets of Fig. 2. Thus, the coupling between mode #0 and a lower order mode (#2) is stronger than that between mode #0 and a higher order mode (#4). The coupling strength can be compared by the coupling constant κ deduced from the coupled-mode theory.¹⁸

$$\kappa_{pq} = (n_{gp} + n_{gq}) \cdot \Delta u_{pq} \cdot \pi/2a. \quad (1)$$

Here, p and q are the two coupled modes, n_{gp} and n_{gq} are group index of mode # p and mode # q , Δu_{pq} is the MSB bandwidth, a is the lattice constant. By our calculation, the coupling constant κ_{02} in DS-PCWG is $0.22a^{-1}$ while κ_{04} for W3 PCWG is only $0.14a^{-1}$ reported in Ref. 18. The large coupling constant of κ_{02} in DS-PCWG indicates an enhanced mode coupling between modes #0 and #2. In order to cause the mode coupling between modes #0 and #2, the range for slot width is within $0.05 \sim 0.7a$ for a fixed r/a of 0.325 and W of $1.4a$. Owing to the enhanced mode coupling of modes #0 and #2, a transmission-dip was obtained in a single DS-PCWG with a length of just $40a$ ($16 \mu\text{m}$), as shown in Fig. 2(b). Obviously, a deep transmission-dip is preferable for obtaining large switching extinction ratio. To achieve it, the DS-PCWG was carefully designed by optimizing the structure parameters. As shown in Fig. 2(b), the extinction ratio of transmission-dip is obtained as high as 30 dB under the optimized parameters of $a=400$ nm, $r=130$ nm, $W_{\text{slot}}=80$ nm, and $W=560$ nm. The transmission-dip under different variations of the refractive index (Δn) was also numerically simulated and shown in Fig. 2(b). It can be seen that the transmission-dip shows a red-shift of 1 nm with $\Delta n=0.002$, which corresponds to temperature variation of 10.75 K with the TO coefficient of $\Delta n/\Delta T = 1.86 \times 10^{-4} \cdot \text{K}^{-1}$ for silicon.⁷

The steady-state thermal analysis was also performed to assess the thermal performance of the proposed switch. 3D finite element method (FEM) is employed to model the temperature distribution and power consumption. The calculated region was fixed as $60 \mu\text{m} \times 60 \mu\text{m} \times 13.3 \mu\text{m}$ to ensure that a room-temperature ($T=293.15$ K) boundary condition is valid at the bottom of the device. The convective cooling boundary was exploited for the other surfaces with a heat transfer coefficient of $5 \text{ W}/(\text{m}^2 \cdot \text{K})$. Varied heating

temperature can be obtained by proper setting the heating power, as given in Fig. 3(a), where the inset is the 3D temperature distribution. The black and red lines are the calculated temperature variations ΔT versus the applied power at the centers of the DS-PCWG and the microheater, respectively. As the temperature increases proportionally to the applied heating power, we define a parameter of heating efficiency η that is the ratio of the ΔT for the DS-PCWG to that of the microheater: $\eta = \Delta T_{\text{PCWG}} / \Delta T_{\text{Heater}}$. In order to analyze the heating efficiency, the vertical temperature distribution under an applied heating power of $P = 2.4$ mW is presented as the black solid curve in Fig. 3(b), while the insets are the top view and cross-section view of the 3D temperature distributions, respectively. The red dotted curve is vertical temperature distribution without the DS-PCWG. It can be seen that the temperature in the DS-PCWG is higher than the area without the DS-PCWG. It is an expected result. Since the DS-PCWG is embedded in a SiO_2 cladding layer, the heat capacity is increased in the holes, and the heat transferring along the DS-PCWG is confined by the SiO_2 layer within the access waveguides. As a result, heating efficiency is increased after introducing the DS-PCWG structure. The heating efficiencies for the Si slab with and without the DS-PCWG are 52.1% and 46.7%, respectively. It is preferable for realizing low power devices.

The switching performance was measured by applying a voltage potential through two electrical probes across the two Al contact pads shown in Fig. 1. Figure 4(a) shows the measured transmission spectra under different heating powers (P). It can be seen that the extinction ratio of the transmission-dip is larger than 20 dB without applying a heating power on our fabricated sample. It is found that the extinction ratio decreases while heating power applied. This is caused by the asymmetric refractive index profile¹⁹ of the upper and lower SiO_2 cladding layer around the DS-PCWG, which can be concluded from the asymmetric temperature distribution in Fig. 3(b). At $P = 9.2$ mW, the central wavelength of the transmission-dip shifted 0.6 nm to longer wavelengths. This red-shift corresponds to ΔT of 6.5 K, which can be calculated from Fig. 2(b) with the silicon TO coefficient. The theoretical heating power to obtain such a temperature variation is 2.4 mW as marked with blue point in Fig. 3(a).

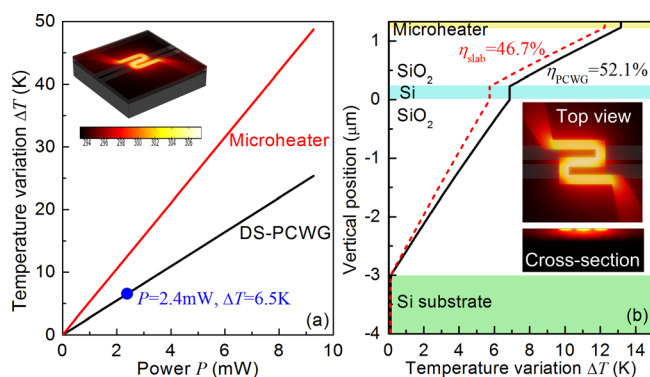


FIG. 3. (a) Temperature variations under different applied heating powers. The inset is the 3D temperature distribution. (b) Temperature distributions located just below the microheater in the vertical direction under an applied heating power of 2.4 mW for the switch. The insets are the top view and the cross-section view for the 3D temperature distribution.

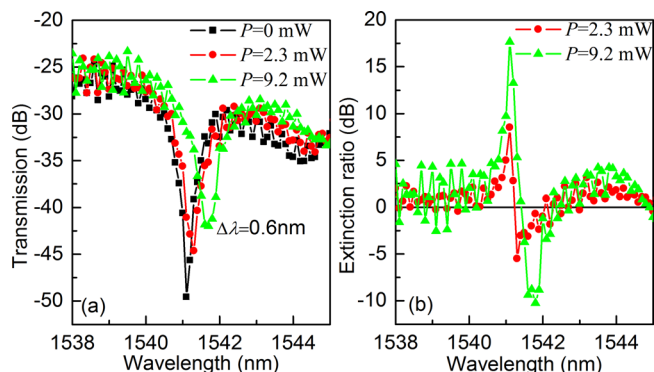


FIG. 4. (a) Measured transmission spectra under different applied heating powers. (b) Extinction ratio of the on- and off-state for the switch.

By choosing a certain wavelength at the transmission-dip, i.e., 1541.1 nm for our fabricated sample, the switch is at the off-state without heating power and turned to the on-state with heating power. The extinction ratios under the heating power of 2.3 and 9.2 mW are shown in Fig. 4(b). The experimental results indicate that extinction ratio as high as 17 dB has been achieved under a switching power as low as 9.2 mW with 16- μm -long DS-PCWG. The thermal tuning efficiency⁹ for our experimental results was 200 pm/2.3 mW and 600 pm/9.2 mW. It should be noted that the simulated thermal tuning efficiency for our proposed device is as high as 600 pm/2.4 mW (250 pm/mW), which shows the potential of high thermal tuning efficiency and provide a promising alternative for the low power and compact devices. Although the double-slot structure in PCWG is not suitable for realizing the *lateral* p-n junction, carrier injection could be achieved by employing a *vertical* p-n junction or a metal-oxide-semiconductor field-effect transistor (MOSFET) type configuration. Thus, the proposed DS-PCWG with the mechanism of enhanced mode coupling in a single PCWG is also potential to achieve high-speed modulation for NoC applications.

In conclusion, an optical switch based on a DS-PCWG with an integrated Ti/Al microheater is demonstrated on SOI substrate. The operating principle is based on shifting a transmission-dip caused by the defect modes coupling in the PBG of the DS-PCWG. Because of the enhanced mode coupling, high extinction ratio of 17 dB has been experimentally achieved under a switching power as low as 9.2 mW while the length of DS-PCWG is only 16 μm .

This work was supported by the National Basic Research Program of China (Nos. 2011CBA00608, 2011CBA00303, and 2010CB327405), the National Natural Science Foundation of China (Grant Nos. 61036011 and 61036010), the Project of Science and Technology on Communication Information Security Control Laboratory, and China Postdoctoral Science Foundation. The authors would like to thank Dr. Fang Liu for his valuable discussions.

¹B. G. Lee, A. Biberman, J. Chan, and K. Bergman, *IEEE J. Sel. Top. Quantum Electron.* **16**, 6 (2010).

²D. Miller, *IEEE Proc.* **97**, 1166 (2009).

³D. M. Beggs, T. P. White, L. Cairns, L. O'Faolain, and T. F. Krauss, *IEEE Photonics Technol. Lett.* **21**, 24 (2009).

- ⁴H. Wen, O. Kuzucu, T. G. Hou, M. Lipson, and A. L. Gaeta, *Opt. Lett.* **36**, 1413 (2011).
- ⁵L. O'Faolain, D. M. Beggs, T. P. White, T. Kampfrath, K. Kuipers, and T. F. Krauss, *IEEE Photonics J.* **2**, 404 (2010).
- ⁶L. L. Gu, W. Jiang, X. N. Chen, and R. T. Chen, *IEEE Photonics Technol. Lett.* **19**, 342 (2007).
- ⁷G. Coppola, L. Sirlito, I. Rendina, and M. Iodice, *Opt. Eng.* **50**, 0711127 (2011).
- ⁸A. Melloni, A. Canciamilla, C. Ferrari, F. Morichetti, L. O'Faolain, T. F. Krauss, R. De La Rue, A. Samarelli, and M. Sorel, *IEEE Photonics J.* **2**, 181 (2010).
- ⁹X. Z. Zheng, I. Shubin, G. L. Li, T. Pinguet, A. Mekis, J. Yao, H. Thacker, Y. Luo, J. Costa, K. Raj, J. E. Cunningham, and A. V. Krishnamoorthy, *Opt. Express* **18**, 5151 (2010).
- ¹⁰Y. A. Vlasov, M. O'Boyle, H. F. Hamann, and S. J. McNab, *Nature (London)* **438**, 65 (2005).
- ¹¹H. C. Nguyen, Y. Sakai, M. Shinkawa, N. Ishikura, and T. Baba, *Opt. Express* **19**, 13000 (2011).
- ¹²X. Wang, C. Lin, S. Chakravarty, J. Luo, A. K. Y. Jen, and R. T. Chen, *Opt. Lett.* **36**, 882 (2011).
- ¹³K. Y. Cui, Y. D. Huang, W. Zhang, and J. D. Peng, *J. Lightwave Technol.* **26**, 1492 (2008).
- ¹⁴M. T. Tinker and J. B. Lee, *Opt. Express* **13**, 7174 (2005).
- ¹⁵Y. H. Cui, K. Liu, D. L. MacFarlane, and J. B. Lee, *Opt. Lett.* **35**, 3613 (2010).
- ¹⁶A. Hosseini, X. C. Xu, D. N. Kwong, H. Subbaraman, W. Jiang, and R. T. Chen, *Appl. Phys. Lett.* **98**, 031107 (2011).
- ¹⁷K. Y. Cui, Y. D. Huang, G. Y. Zhang, Y. Z. Li, X. Tang, X. Y. Mao, Q. Zhao, W. Zhang, and J. D. Peng, *Appl. Phys. Lett.* **95**, 191901 (2009).
- ¹⁸S. Olivier, H. Benisty, C. Weisbuch, C. Smith, T. Krauss, and R. Houdre, *Opt. Express* **11**, 1490 (2003).
- ¹⁹B. S. Song, S. W. Jeon, and S. Noda, *Opt. Lett.* **36**, 91 (2011).